Fresh volcanic aerosols injected in the atmosphere during the volcano eruptive activity at the Cumbre Vieja area (La Palma, Canary Islands): Temporal evolution and vertical impact

Carmen Córdoba-Jabonero, Michaël Sicard, África Barreto, Carlos Toledano, María Ángeles López-Cayuela, Cristina Gil-Díaz, Omaira García, Clara Violeta Carvajal-Pérez, Adolfo Comerón, Ramón Ramos, et al.

Fresh volcanic aerosols injected in the atmosphere during the volcano eruptive activity at the Cumbre Vieja area (La Palma, Canary Islands): Temporal evolution and vertical impact

Carmen Córdoba-Jabonero[1*], Michaël Sicard[2,3#], África Barreto[4], Carlos Toledano[5], María Ángeles López-Cayuela[1], Cristina Gil-Díaz[2], Omaira García[4], Clara Violeta Carvajal-Pérez[1], Adolfo Comerón[2], Ramón Ramos[4], Constantino Muñoz-Porcar[2], and Alejandro Rodríguez-Gómez[2]

[1]Atmospheric Research and Instrumentation Branch, Instituto Nacional de Técnica Aeroespacial (INTA), Torrejón de Ardoz, Spain
[2]CommSensLab, Dept. of Signal Theory and Communications, Universitat Politècnica de Catalunya, Barcelona, Spain
[3]Ciències i Tecnologies de l'Espai-Centre de Recerca de l'Aeronàutica i de l'Espai/Institut d'Estudis Espacials de Catalunya (CTE-CRAE/IEEC), Universitat Politècnica de Catalunya, Barcelona, Spain
[4]Izaña Atmospheric Research Center, State Meteorological Agency of Spain (AEMET), Izaña, Spain
[5]Group of Atmospheric Optics, Universidad de Valladolid, Spain
[#]Now at: Laboratoire de l'Atmosphère et des Cyclones (LACy), Université de La Réunion, Saint Denis, France

*Corresponding author: Carmen Córdoba-Jabonero, cordobajc@inta.es, Instituto Nacional de Técnica Aeroespacial (INTA), Atmospheric Research and Instrumentation Branch, Ctra. Ajalvir, km. 4, Torrejón de Ardoz-28850 (Madrid), Spain

Abstract. For the first time in fifty years, the Cumbre Vieja volcanic area (La Palma, Canary Islands, Spain) erupted on 19 September 2021, giving birth to a new volcano. Fresh volcanic aerosols were continuously injected into the troposphere at different height levels, decreasing with time until the end of December 2021 (15 weeks duration). A wide set of different instrumentation was deployed all over the Island in order to evaluate the effects of the volcanic plumes on the atmosphere and the air quality. For the first time, a long-term study of the relative mass contribution and vertical impact of the volcanic components, ash and non-ash particles separately, during the eruptive activity was carried out in this work. In particular, a polarized Micro-Pulse Lidar (P-MPL) was deployed at Tazacorte (at around 8 km west from the volcano) in 24/7 operation from 17 October 2021 until the end of the volcano activity (11 weeks) for vertical monitoring of the volcanic particles. First, a statistical study of the mass conversion factors for mass concentration estimation of the volcanic (ash and non-ash) particles was performed by using the AERONET sun/sky-photometer dataset at Fuencaliente (at around 18 km south from the volcano). A representative mass conversion factor was obtained for ash and non-ash particles: 1.89 ± 0.53 and 0.31 ± 0.06 g m^{-2}, respectively, with no dependence on time and optical depth. Second, these factors were used to calculate the ash and non-ash mass concentrations from P-MPL observations. Ash particles dominated 11% of the time and mostly until week 3 (i.e. week 7 from the volcanic eruption). Their mass concentration decreased by one order of magnitude: the relative ash mass contribution was 73 ± 18% with a total mass loading of 566 ± 281 mg m^{-2} at week 1, reducing gradually down to 38 ± 32% and 120 ± 49 mg m^{-2}, respectively, at week 11. Layer-to-layer, it decreased with increasing layer-height; no ash was detected above 4 km at the end of the volcanic period. Third, in order to analyse the potential AERONET underestimation of the coarse mass conversion factor due to the 15 μm cutoff effect in the AERONET retrieval, two worst-case-scenarios (WCS) were examined, representing aged-like ash particles (WCS1, 4-μm radius) and fresh-like (WCS2, 10-μm radius). For both scenarios, the mass concentration of the volcanic plumes exceeded the first contamination level (> 200 μg m^{-3}, as defined by the UK Meteorological Office) up to 5-6 km height mostly during week 1 and up to 1-2 km until week 9. The extreme contamination level (> 2000 μg m^{-3}, aircraft flight limitations) was only exceeded from week 1 to week 6 under WCS2 conditions. This work infers a new long-term insight on the volcanic matter injected in the atmosphere with relevance for Air Quality issues and air traffic safety policies.

Keywords: Mass conversion factors; Polarized Micro-Pulse Lidar; Remote sensing; Sun/sky photometer; Cumbre Vieja volcano; Volcanic ash.

Citation. Córdoba-Jabonero, C., Sicard, M., Barreto, Á., Toledano, C., López-Cayuela, M. Á., Gil-Díaz, C., García, O., Carvajal-Pérez, C. V., Comerón, A., Ramos, R., Muñoz-Porcar, C., and Rodríguez-Gómez, A., 2023. Fresh volcanic aerosols injected in the atmosphere during the volcano eruptive activity at the Cumbre Vieja area (La Palma, Canary Islands): Temporal evolution and vertical impact. Atmospheric Environment, 300, 119667. https://doi.org/10.1016/j.atmosenv.2023.119667.

1. Introduction

It is widely known that volcanic aerosols, mainly composed of ash particles and fine particulate matter (sulphates, mainly), play an important role in the energy balance of the atmosphere, affecting the surface temperature and inducing the formation of clouds, and hence in the climate (e.g. Robock, 2000; Robock and Oppenheimer, 2003; and references therein). At local scale, volcanic aerosols can affect greatly the air quality and health issues (e.g. Colette et al., 2011; Stewart et al., 2021), but also air traffic, as it drastically occurred when the Icelandic Eyjafjallajökull volcano erupted in 2010, which triggered the complete airspace closure in Europe yielding socio-economic concerns (Volcanic Ashfall Impact Working Group; https://volcanoes.usgs.gov/volcanic_ash/ash_clouds_air_routes_eyjafjallajokull.html, last access: 2 February 2023) and health issues (Icelandic Directorate of Health; https://www.landlaeknir.is/english/annual-reports/, last access: 25 January 2023). On those concerning days, several scientific, but not only, initiatives started with a focus on monitoring and investigating the transport and evolution of volcanic aerosols. In this point, it should be highlighted the excellent aptitude of the existing aerosol remote sensing networks, like AERONET (Aerosol Robotic Network; Holben et al., 1998), EARLINET (European Aerosol Research Lidar Network; Pappalardo et al., 2014), and MPLNET (NASA Micro-Pulse Lidar Network; Welton et al., 2001), among others, to dedicate a great scientific effort for that purpose. Besides, their aerosol observations served to show the weakness of dispersal simulations of the volcanic plumes by the forecast models at that moment. In general, a relevant advance in the study of volcanic aerosols and their risks for the life in overall was achieved by accounting with the experience of carrying out an exhaustive observational monitoring by using remote sensing instrumentation from ground-based stations (e.g. Gasteiger et al., 2011; Kokkalis et al., 2013), including specially lidar systems (e.g. Mattis et al., 2010; Ansmann et al., 2011, 2012; Hervo et al., 2012; Mona et al., 2012; Papayannis et al., 2012; Pisani et al., 2012; Scollo et al., 2012; Sicard et al., 2012; Navas-Guzmán et al., 2013), from satellite-based platforms (e.g. Prata and Prata, 2012; Prata et al., 2017), and from both of them (Sawamura et al., 2012; Toledano et al., 2012; Lopes et al., 2019; Sannino et al., 2022).

In this framework, when the new volcano at the Cumbre Vieja Natural Park (named Cumbre Vieja volcano hereafter) of the La Palma island (Canary Islands) erupted on 19 September 2021 (Longpré, 2021), a huge scientific effort of collaboration within ACTRIS (Aerosol, Clouds and Trace Gases Research Infrastructure) and ACTRIS-Spain (https://actris.es.webstsc.webs.upc.edu/en/node/11, last access: 17 December 2021) was promptly carried out, being led by the Spanish Agencia Estatal de Meteorología (AEMET) together with several Canary public institutions (regional, insular and local governments) (García et al., 2022). Indeed, several research groups and other organizations, mainly from Europe, deployed scientific instrumentation to the area of the eruption in order to study the evolution and transport of the fresh volcanic aerosols emitted to the atmosphere.

The volcanic eruption, with large amounts of fresh particulate matter ejected to the atmosphere and perturbing lava flows, triggered the extreme evacuation of the population, the cancelation of hundreds of flights, the destruction of many infrastructures and serious damage to the island crops, among other damages. From a socio-economic point of view, this set of disasters produced a final balance of damages estimated to 842 M€ (Europa Press, https://www.europapress.es/islas-canarias/noticia-canarias-remite-gobierno-evaluacion-danos-volcan-palma-84233-millones-20211204160648.html; last access: 28 Dec. 2021.). Moreover, the volcano activity was monitored by the PEVOLCA (Plan Especial de Protección Civil y Atención de Emergencias por Riesgo Volcánico en la Comunidad Autónoma de Canarias; https://info.igme.es/eventos/Erupcion-volcanica-la-palma/pevolca, last access: 17 December 2021), designating the Cumbre Vieja eruption (Strombolian type) with a volcanic explosivity index (VEI) of 3 (moderate) (Newhall and Self, 1982). The eruptive release of fresh particulate matter lasted until 13 December 2021 (nearly 3 months duration), being the volcanic eruption at the Cumbre Vieja Natural Park stated concluded at the end of December 2021 (PEVOLCA).

In particular, within the overall interest in the implications of the Cumbre Vieja volcanic eruption at La Palma Island as a whole, a special emphasis was devoted to the study of the ash particles in terms of their vertical distribution with respect to the fine (non-ash) particulate matter. Indeed, the characterization of the optical properties of fresh ash particles and their concentration levels is one of the main concerns nowadays. In fact, limitations in their concentration were stated after the eruption of Eyjafjallajökull volcano in 2010 in relation to the first contamination level as defined by the UK Meteorological Office (limited to 200 μg m^{-3}, International Civil Aviation Organization (ICAO); Schumann et al., 2011), and the maximal concentration acceptable for regular aircraft flights (up to 2000 μg m^{-3}, International Civil Aviation Organization (ICAO); Schumann et al., 2011). As stated before, the use of aerosol active remote sensing observations, in particular polarized lidar systems, has demonstrated being of great relevance for the study of the properties of volcanic aerosols, either aged (e.g. Ansmann et al., 2011; Gasteiger et al., 2011; Sicard et al., 2012) or fresh particles (e.g. Pisani et al., 2012; Scollo et al., 2012).

However, those studies were focused on single or very short-term (a few days) case studies . The eruption of the Cumbre Vieja volcano provided the opportunity to investigate the potential changes in the properties of the ash particles, highlighting the 'fresh' state of these particles (detected at less than 10 km from the volcano), under long-term volcanic conditions. For that purpose, among the extensive instrumental deployment made over La Palma Island for the volcano environment research, polarized lidar and sun-photometer measurements were continuously carried out at two strategic sites nearby the Cumbre Vieja volcano (at least for the availability period of remote sensing measurements).

A first insight into the results obtained from long-term observations of the Cumbre Vieja volcanic particulate matter injected into the atmosphere was presented by Sicard et al. (2022). They examined the optical properties (particle backscatter coefficient, particle depolarization ratio) of the ash particles, which presented depolarization ratios slightly lower (0.20-0.30) than those found after the Eyjafjallajökull volcano eruption for aged ash particles (0.35-0.40) (e.g. Ansmann et al., 2011; Gasteiger et al., 2011; Sicard et al., 2012). In addition, several studies on fresh ash particles from the eruption of the Mount Etna volcano (Pisani et al., 2012; Scollo et al., 2012) reported both moderate (0.16) and high (0.45) depolarization ratios. Two more studies about the Cumbre Vieja eruption have been published so far: Bedoya-Velásquez et al. (2022) studied the spatio-temporal variability with 2 AERONET photometers and 3 ceilometers located in the island, while Milford et al. (2023) studied the volcanic impact on air quality. Cumbre Vieja eruption was dominated by a Strombolian basaltic activity, but some periods with effusive activity and violent ash-rich explosions were also detected. Another feature of this eruption was the considerable low plume height, with an average value of about 3500 m a.g.l. (Felpeto et al., 2022). This low plume height is a critical factor for the air quality impact on surface, as reported by Milford et al. (2023).

In this work, for the first time, a long-term study of the volcanic ash and non-ash particles, separately, during the eruptive activity was carried out. Their evolution and final decay, with the focus on determining their relative mass contribution, was examined in detail along the Cumbre Vieja volcano activity. In addition, the vertical mass impact of ash particles, related to the established limitation of their mass concentration levels, was also analysed. The work is structured as follows: **Section 2** introduces the methods, describing the measurement stations, the instrumentation, and the methodology used; **Section 3** includes the results, disclosed in the estimation of representative mass conversion factors for ash and non-ash particles, the evolution of their volcanic mass concentration, and the volcanic impact in the troposphere under two worst-case scenarios (WCS); finally, **Section 4** presents the conclusions.

2. Methods

2.1 Measurement sites and instrumentation

Volcanic plumes were continuously monitored by using remote sensing instrumentation at two sites, strategically located from the Cumbre Vieja volcano (1120 m a.s.l.) emissions. **Figure 1** shows the geographical

composition of the volcanic eruption area in the Cumbre Vieja Natural Park at La Palma (Canary Islands), including the two measurements sites (Tazacorte and Fuencaliente), and the position of the La Palma airport, together with their relative distances.

A polarized Micro-Pulse Lidar (P-MPL; v. MPL-4B, Droplet Measurement Technologies LLC, Longmont, CO, USA), operated by the Polythecnic University of Catalonia (UPC) and the Spanish Institute for Aeroespace Technology (INTA), was deployed in Tazacorte (28.6ºN, 17.9ºW, 140 m a.s.l.), on the west coast of the island, at around 8 km west from the volcano (see **Fig. 1**), and operated from 17 October 2021 until the end of January 2022. The P-MPL measurement period considered in this study is from 17 October to 31 December 2021 (11 weeks) as the volcanic activity was drastically reduced by the end of December 2021. The P-MPL system is an eye-safe elastic single-wavelength lidar with a relatively high pulse repetition frequency (2500 Hz), a low-energy (6-8 μJ) Nd:YVO4 laser at 532 nm, and depolarization capabilities. It operates in full-time continuous mode (24/7), performing measurements with 1-min integrating time and 75-m vertical resolution. A complete description of the data correction and calibration processing can be found in several works (e.g. Campbell et al., 2002; Welton and Campbell, 2002; Flynn et al., 2007; Córdoba-Jabonero et al., 2021). The primary P-MPL data are the total range-corrected signal (RCS) and the volume linear depolarization ratio (VDR), which enable obtaining height-resolved aerosol optical and microphysical properties by using different retrieval algorithms and methods (see **Sect. 2.2**). In particular, the particle depolarization ratio (PDR, δ_p), and both the particle backscatter (β, Mm^{-1} sr^{-1}) and extinction (σ, Mm^{-1}) coefficients together with the particle mass concentration (m, μg m^{-3}) for both volcanic ash (coarse) and non-ash (fine) aerosols were analysed (see **Sect. 2.2**).

The closest AERONET station to Tazacorte, where the P-MPL was deployed, is "La Palma" site at Fuencaliente (28.5ºN, 17.9ºW, 630 m a.s.l.), which is located at the south of the island, at 18 km far from the volcano and 21 km southeast distance from Tazacorte (see **Fig. 1**). This AERONET site was set up by the University of Valladolid and AEMET to monitor the volcanic aerosols during the eruptive period. A sun/sky photometer (CE-318T, Cimel Electronique, Paris, France), which operated from 22 September 2021 on, was used for statistically estimating the mass conversion factors (see **Sect. 3.1**), which were applied together with the extinction profiles as retrieved from the P-MPL measurements to obtain the mass concentration of both volcanic ash and fine aerosols (see **Sect. 2.2**). AERONET inversion products V3 L1.5 (AERONET, https://aeronet.gsfc.nasa.gov; last access: 17 January 2022) were used (unfortunately, AERONET V3 L2.0 data were not available at that moment), in particular, the columnar volume concentrations (v, μm^3 μm^{-2}) and the aerosol optical depths at 500 nm (τ) for the coarse and fine modes. Note that AERONET retrievals are more restrictive for deriving v than τ, being thus reduced the number of simultaneous v and τ values (Giles et al., 2019; Sinyuk et al., 2020). For instance, 356 hourly τ values in comparison with 103 hourly v values (that is, 29% with respect to those τ) were derived.

2.2 Methodology

The methodology is two-fold and consists on: 1) the statistical analysis of the AERONET sun/sky photometer data to derive a specific columnar-equivalent mass conversion factor for each of the volcanic coarse (ash) and fine (non-ash) components; and 2) the data processing applied to the P-MPL measurements, which was performed exclusively with validated in-house algorithms (Flynn et al., 2007; Córdoba-Jabonero et al., 2018), to retrieve the profiles of both the extinction coefficient and mass concentration for ash (coarse-predominant component) and non-ash (fine component) aerosols, separately.

Lidar measurements were hourly-averaged, resulting in 1824 1-h RCS and VDR profiles for the overall measurement period (17 October - 31 December 2021, 76 days, 11 weeks). However, for a determined number of profiles the volcanic plume was dense enough to screen the lidar signal; additionally, condensation issues, particle deposition, and other technical problems prevented the signal collection. Disregarding all of them, 84.2% out of the total number of 1-h RCS profiles (i.e. N=1535) were considered for the retrieval of optical properties. Indeed, those 'valid' profiles were used for deriving both the total β_p and PDR profiles by applying the Klett-Fernald method (Fernald, 1984; Klett, 1985) with a lidar ratio of 50 sr. The POlarisation LIdar

PHOtometer Networking (POLIPHON) algorithm was used to separate the total β_p into their fine- and coarse-mode components on the basis of the PDR profiling, and estimate their mass concentration (e.g. Ansmann et al., 2011, 2012). In particular, POLIPHON was applied successfully to P-MPL measurements for different aerosol mixtures (Córdoba-Jabonero et al., 2018). In this work, the separation of the volcanic particulate matter into two aerosol components is achieved: ash particles (*a*), which are assumed the coarse-dominating aerosol, and non-ash particles (*na*), which correspond to the fine-mode of the volcanic aerosols (mainly sulphates). This method is based on the attribution of specific values of the PDR (δ), lidar ratio (S) and mass conversion factors (f_m) to both *a* and *na* components (Ansmann et al., 2011, 2012).

In summary, the POLIPHON retrieval is performed in the following steps:

1) Separation of the P-MPL total backscatter coefficient (β_p) into their *a* and *na* modes, i.e. $\beta_p = \beta_a + \beta_{na}$.

The optical properties were examined in Sicard et al. (2022), where two case studies were specially analyzed. Despite the scope of the present work is mainly focused on the mass concentration assessment of the volcanic aerosols, for the sake of illustrating their evolution in terms of their optical properties, **Figure 2** shows the vertical β_p and δ_p (PDR) along the P-MPL observational period until the end of the volcanic activity (11 weeks, from 17 October to 31 December 2021). Unfortunately, Saharan dust episodes were detected (see Milford et al., 2023 for details) within the first and last weeks (mainly on 19-21 October and 30 December, as denoted by light brown bands in **Fig. 2**), contaminating thus the volcanic mixtures; hence, those two dusty episodes were discarded from the study. It should be noted that the maximal weekly values (δ_p^{max}) were ranging from 0.22 to 0.34 at altitudes ($Z(\delta_p^{max})$) between 1.1 and 2.9 km height. On average for the whole period, a mean hourly δ_p of 0.25 ± 0.04 is obtained together with a mean $Z(\delta_p^{max})$ value of 2.4 ± 0.5 km (see **Fig. 2**). This can infer a moderate mixing between ash (high depolarizing) and non-ash (low depolarizing) particles, since higher δ_p values would be expected by looking at those reported for other volcanic eruptions; for instance, Ansmann et al. (2011) provided representative values of 0.36 for ash, being the reference δ_p value for volcanic ash used in this work (see **Table 1**).

2) Calculation of the mass concentration (m, g m^{-3}) for both *a* and *na* modes, as follows

$$m_i = \beta_i \, S_i \, {f_m}^i \,, \quad (1)$$

being ${f_m}^i$ the mass conversion factor (g m^{-2}), which is defined as

$${f_m}^i = {f_v}^i \, \rho_i, \quad (2)$$

where ${f_v}^i$ is the volume conversion factor (10^{-12} Mm), ρ_i is the particle density (g cm^{-3}), and i denotes *a* and *na* components.

Lidar ratio estimates of just erupted volcanic aerosols in the Cumbre Vieja volcanic area were not available. Ansmann et al. (2011) reported S values of 50 and 40-80 sr, respectively, for aged Eyjafjallajokull volcanic ash and non-ash aerosols, being the estimated error within 10-30%. Similar values were obtained for those Eyjafjallajokull volcanic plumes as detected along their pathway (e.g. Mona et al., 2012). However, Pisani et al. (2012) obtained lidar ratios of 36 ± 5 and 46 ± 10 sr, respectively, for fresh volcanic coarse and fine aerosols from the Mt. Etna eruption, but corresponded to particular volcanic layers in single days. By looking at those reported lidar ratios, the discrepancies observed, likely due to the different eruptive style of each volcano and the potential variations of the volcanic particles during their long- or short-range transport, are within their associated errors. Therefore, S values of 50 sr were assumed for each volcanic component in this work (see **Table 1**), as also used in Ansmann et al. (2011) who studied a large number of measurements at various sites of Eyjafjallajokull volcanic cases. In this sense, additional analysis on the differences in the extinction (and then in the mass) between components in relation to the assumed lidar ratio is disregarded in this work.

Conversion factors f_v can be determined from the AERONET columnar volume concentration (v) and aerosol optical depth (τ) products (e.g. Ansmann et al., 2011, 2012) for both the fine and coarse modes, i.e. ${f_v}^i =$

v_i/τ_i; note that i = *a* (coarse) and *na* (fine), as stated before. Unfortunately, AERONET data were unavailable at Tazacorte, where P-MPL observations were performed. Therefore, f_v were derived from the AERONET data available from the Fuencaliente sun/sky photometer (the closest site to Tazacorte; see **Sect. 2.1**). However, the distance between Tazacorte and Fuencaliente sites was relatively long (i.e. 21 km far from each other; see **Fig. 1**), which makes questionable the use of the conversion factors obtained in Fuencaliente to data obtained in Tazacorte. Indeed, meteorological variables such as the wind direction and intensity, among others, can likely affect the volcanic situation at both sites, leading to different conditions and thus to potentially biased retrievals of the mass properties of the volcanic aerosols in Tazacorte. For that reason, a statistical analysis of the AERONET data (i.e. v and τ) at Fuencaliente along the overall observational P-MPL period was performed in order to obtain representative f_v values for both *a* and *na* components to be used for mass concentration estimation from the P-MPL measurements in Tazacorte. A columnar effective mass conversion factor ${f_v}^{eff} = \overline{v/\tau}$ for both coarse and fine modes, which is representative of *a* and *na* components (as stated before), respectively, was computed. The degree of representativeness of those statistically computed conversion factors will be discussed in **Sect. 3.1**. **Table 1** shows all the POLIPHON input values used in this work.

Once determined the mass conversion factors f_m for each component (see **Table 1**), the mass concentration profiles m for *a* and *na* components (see **Eq. 1**) were derived along the P-MPL measurement period. Uncertainties in the mass concentrations m_a and m_{na} of 40% and 35-60%, respectively, were computed on the basis of the relative uncertainties in β_p (for a; na: 10-15%; 10-40%), from the assumption of S (10%; 25%) and ρ (15%; 15%) values (Ansmann et al., 2012), and in those obtained f_v (30%; 20%; see **Sect. 3.1**). In addition, height-integrated mass concentrations (i.e. mass loadings M, g m^{-2}) were obtained for each component, as follows

$$M_i = \sum_z m_i(z)\,\Delta z, \quad (3)$$

where z denotes the height-dependence, Δz is the lidar vertical resolution, and i = *a*, *na*. The total mass loading M^{total} is then

$$M^{total} = M_a + M_{na}, \quad (4)$$

being M_a and M_{na} the mass loadings of ash and non-ash particles, respectively. From **Eq. 4** the relative contribution of each component to the total mass loading (i.e. the mass fraction for i = *a*, *na*, in %) can be easily computed, that is,

$$M_i^{rel} = 100 \times M_i/M^{total}. \quad (5)$$

3. Results and discussion

3.1 Estimation of representative mass conversion factors for ash and non-ash particles

As stated in **Section 2**, AERONET retrieval of the volume concentrations (v) is more restrictive than the one of the aerosol optical depth (τ); hence, the availability of v values limited the number of conversion factors to be computed. Therefore, simultaneously available both AERONET v and τ values were daily-averaged, and used for deriving the mass conversion factors f_m (see **Eq. 2** and **Table 1**), obtaining 41 daily values for the period between 22 September (starting of the sun/sky photometer measurements) and 31 December 2021. The time series of the daily-averaged f_v (= v/τ) of the fine and coarse modes for the total Fuencaliente AERONET dataset for that whole period is shown in **Figure 3**.

The representativeness of the f_v values for each of the volcanic components is obtained from the statistical analysis of both time series. Looking at **Figure 3**, the dispersion of the ${f_v}^a$ is greater than that for ${f_v}^{na}$ (as previously commented, note that *a* will be denoted by 'coarse' and *na* for 'fine' hereafter, for similarity taking into account AERONET particle modes). That can be confirmed by calculating the mean $\pm$ standard deviation (relative deviation) values of the complete AERONET-derived fine and coarse f_v datasets, that is, $\overline{{f_v}^{fine}}$ = 0.204 $\pm$ 0.041 10^{-12} Mm (20.3%), and $\overline{{f_v}^{coarse}}$ = 0.726 $\pm$ 0.202 10^{-12} Mm (27.8%). By considering the period starting from the P-MPL measurements (17 October 2021 on), despite the number of daily f_v values is reduced down

to 23, those values are rather similar (only around 2% lower): $\overline{f_v^{fine}}$ = 0.200 ± 0.047 10^{-12} Mm, and $\overline{f_v^{coarse}}$ = 0.710 ± 0.234 10^{-12} Mm, although the dispersion is slightly higher (23.7 and 33.0%, respectively).

Regarding f_v^{coarse}, which presents an enhanced dispersion, it was examined in comparison with τ^{coarse}, as shown in **Figure 4**. It can be easily noted that the behaviour of f_v^{coarse} is quite variable for τ^{coarse} < 0.1: this is confirmed by computing $\overline{f_v^{coarse}}$ in those two τ^{coarse} intervals: $\overline{f_v^{coarse}}$ = 0.728 ± 0.211 10^{-12} Mm (28.9%, N=35) for τ^{coarse} < 0.1, and $\overline{f_v^{coarse}}$ = 0.715 ± 0.139 10^{-12} Mm (19.4%, N=6) for τ^{coarse} ≥ 0.1. Those values are just +0.3 and -1.5% different, respectively, from those computed for the whole period of the AERONET dataset obtained from the sun/sky photometer measurements as performed at Fuencaliente. Indeed, these results show that, overall, mean f_v^{coarse} values are neither time- nor τ^{coarse}-dependent.

Therefore, the representative values used in this work for the *na* (non-ash) and *a* (ash) components were both f_v^{fine} = 0.204 10^{-12} Mm and f_v^{coarse} = 0.726 10^{-12} Mm (**Table 1**), respectively. By computing the corresponding mass conversion factors f_m (g m^{-2}) using the particular ρ for each volcanic component (see **Table 1**), f_m^{na} = 0.31 ± 0.06 g m^{-2} and f_m^{a} = 1.89 ± 0.53 g m^{-2} were obtained, which were applied to derive the mass concentrations profiles of both the *a* and *na* particles. Those f_v and f_m values are also included in **Table 1**.

Note that these f_v values were 15% (*na*) and 20% (*a*) larger than the corresponding values found in Ansmann et al. (2011) as observed for a volcanic plume transported for 2-3 days. This is a likely outcome, as large-to-giant particles are expected to be present in fresh volcanic plumes, producing an almost linear increase in f_v^{coarse} (Gasteiger et al., 2011; Schumann et al., 2011). However, the properties of the particles with radii larger than 15 μm cannot be retrieved by the AERONET inversion algorithm, which may produce an underestimation of the coarse-mode v, and, thus, of f_v^{coarse}. In order to consider this potential limitation, f_v^{coarse} was also computed for two assumed maximal effective radii (r_{eff}, μm) for the coarse mode. That is, r_{eff} of 4 μm, as considered in Schumann et al. (2011) and Ansmann et al. (2011) for aged-like volcanic particles, and 10 μm, as in Pisani et al. (2012) for fresh ash, were selected to estimate f_v^{coarse} following the linear relationship $f_v^{coarse} = {}^{2\,r_{eff}}/_{3}$ proposed by Ansmann et al. (2011) for size distributions dominated by large-to-giant particles. AERONET reported r_{eff} values for the fine and coarse mode of 0.15 ± 0.02 μm and 1.97 ± 0.38 μm, respectively, on average for the whole period. In the case of the coarse mode, those assumed r_{eff} of 4 and 10 μm in the worst-case-scenarios (WCS) were, respectively, around 2 and 5 times higher than the AERONET ones. As a result, the two maximums of f_v^{coarse} were estimated to be 2.67 10^{-12} and 6.67 10^{-12} Mm, respectively, i.e. 3.7 and 9.2 times larger than the AERONET-derived f_v^{coarse}. In order to investigate this issue in particular, other potential changes in the size of the volcanic ash related to the f_v^{coarse} (and then to the mass) increase, as for instance the water uptake by the volcanic ash (Ansmann et al., 2011; Lathem et al., 2011), were ignored.

Therefore, in the case of fresh ash particles emitted by the Cumbre Vieja volcano at around 8 km away from Tazacorte (P-MPL observations), two WCS in terms of their mass concentration injected in the troposphere were considered by using the AERONET-derived f_v^{coarse} (see **Table 1**) multiplied by 3.7 (WCS1) and 9.2 (WCS2). This corresponded to a similar enhancement of the ash mass concentration, being the total mass concentration strongly dominated by the contribution of the ash particles. Those two WCS can reflect the different mass impact of ash particles under volcanic aged-like (i.e. WCS1) and fresh-like (i.e. WCS2) conditions, respectively. This point will be examined in detail later in **Section 3.3**.

3.2 Evolution of the volcanic mass concentration

Once determined the mass conversion factors f_m for each component (see **Table 1**), the methodology as described in **Section 2.2** was applied to retrieve the mass concentration m profiles for *a* and *na* components (see **Eq. 1**) and the relative fraction of each component to the total mass loading (see **Eq. 5**). **Figure 5** shows the evolution of the relative mass contribution (M^{rel}, %) to the total mass loading of both ash (M_a^{rel}) and non-

ash (M_{na}^{rel}) particles together with the total mass loading (M^{total}, mg m^{-2}) along the overall P-MPL measurement period (**Fig. 5a**), highlighting the time intervals when the condition of M_a^{rel} > 80%, and also the less restrictive condition of M_a^{rel} being between 40 and 60%, is fulfilled (**Fig. 5b**).

The overall impact of ash particles on the troposphere is examined in terms of the time percentage with respect to the overall P-MPL measurement period when M_a^{rel} fulfilled that restrictive condition of being higher than 80% (and also in the 40-60% range, although it is less restrictive). Results indicated that around 11% out of the full period (11 weeks of P-MPL observations) the troposphere was dominated by ash particles (M_a^{rel} > 80%). That time percentage increased up to 35.2% by considering that the mass fraction of ash particles was similarly balanced with that for the volcanic fine (non-ash) aerosols (i.e. M_a^{rel} = 40-60%). All those values are shown in **Table 2**. By looking at **Figure 5b**, brown bands (M_a^{rel} > 80%) were most frequent within the week 1, 3-4 and 7-8, meanwhile the purples ones (M_a^{rel} = 40-60%) were widely found until the beginning of the week 9. From the middle of week 9 on, a drastic reduction of the ash particles (M_a^{rel} < 20%) was obviously observed (disregarding the last days of the period, likely affected under dusty conditions).

As expected, this particular behaviour is also observed in the evolution of M^{total} (see **Fig. 5a**, hourly values), since, as stated before, the total mass concentration is strongly dominated by the contribution of the ash particles. By looking at the daily and weekly tendency (see **Fig. 5a**, magenta and cyan lines, respectively), a gradual decreasing drift, close to an exponential decay (the right Y axis being in log scale), was observed in both trends along the whole period. Hence, this M_a reduction was calculated by the ratio (γ, in %) between the weekly-averaged M_a values as obtained at the end of the volcano activity (i.e. in week 11) with respect to the beginning of the observational P-MPL period (week 1). In particular, the weekly M_a values were 442 and 43 mg m^{-2}, on average, within the week 1 and 11 (once dusty days discarded), respectively; hence, γ represented a 9.8% in M_a reduction (see **Table 2**). Regarding those values under the WCS conditions, M_a reached 1635 $\pm$ 1061 (WCS1) and 4065 $\pm$ 2639 (WCS2) mg m^{-2} at the beginning of the observational period (week 1), with the same expected reduction ratio (γ = 9.8%) until week 11. In addition, even under the nominal volcanic scenario (NVS, representing no mass enhancement), the mass loading of ash particles in the troposphere overcame 1000 mg m^{-2} a few times (11 in total) only, mainly between the week 1 and 3 (8 times), reaching a maximum of 1790 mg m^{-2} (NVS).

In order to examine the vertical impact of the volcanic particulate matter injected to the troposphere, the relative mass contribution of both ash and non-ash components for all the period was also computed in height-intervals of 1 km thick (L layers) up to 6 km height (for instance, L1 denoted the 0-1 km layer). This is shown in **Figure 6**, where from the top to bottom and from the left to rights panels, the contribution of both the ash and non-ash components is represented in each L layer (L1-L6). In addition, the hourly- and weekly-averaged M^{total} values are included, mainly in order to vertically represent the mostly descending trend of the volcanic mass loading.

The layer-to-layer impact of ash on the troposphere with respect to the entire duration of the volcano activity was also examined, likewise for the atmospheric column, and results are shown in **Table 2**. The volcanic conditions with dominance of ash particles (i.e. M_a^{rel} > 80%) were present 11-15% out of the overall time at the L1-L3 layers (see **Figs. 6a-6c**), being maximal (14.6%) in the L2 layer (1-2 km height, just above the volcano altitude). From L4 to L6 layer (see **Figs. 6d-6f**), that time percentage was drastically reduced (from 7 to 2%), confirming that volcanic ash reached mostly altitudes lower than 3 km height. The volcanic conditions with a well-balanced situation between ash and non-ash particles (i.e. M_a^{rel} = 40-60%) had a rather similar behaviour in all first three layers (time percentage ~25-26% in the L1-L3 layers) and also drastically decreased in layers L4 up to L6 (from 12.4 to 0.9%). Note that no ash particles were mostly detected at the L5 and L6 layer for the second half of the P-MPL observational period; hence, it should be highlighted that results are conditioned, showing that the time when M_a^{rel} > 80% is fulfilled is twice to the less restrictive conditions (40-60%), i.e. 3.8 to 1.9% at L5 and 1.9 to 0.9% at L6 (see **Table 2**).

Moreover, as expected, that particular descending behaviour is also observed in the evolution of M^{total} at each L1-L4 layer until the end of the observational period (see **Figs. 6a-6d**, hourly values), since, as stated before, the total mass concentration is strongly dominated by the contribution of the ash particles. At the highest L5 and L6 layers, they were just observed in sporadic episodes, and definitively were undetected at L5 from week 9 and at L6 from week 7 onward (see **Figs. 6e-6f**). This confirms, as stated before, the presence of ash particles mainly up to 3-4 km height (in particular, they were drastically vanished at L4 from week 4 on).

Indeed, by looking at the weekly tendency (see **Figs. 6a-6d**, cyan lines), a gradual decreasing drift (likely close to an exponential decay) was observed at all L1-L4 layers along the whole period. This no-lineal decrease is anticorrelated with the height of the lowermost ash layer which was increasing until week 7 (Sicard et al., 2022), and it is correlated with, and probably enhanced by, the decrease of the height of the lowermost ash layer after week 7 (see **Figs. 6b-6c**). Note also that the no-lineal decrease of the mass concentration is enhanced with increasing layer-height. This is well represented by the reduction ratio between week 11 and 1, which decreases with increasing layer, i.e. from γ = 18.7% between the surface and 1 km height (L1) until almost zero at 3-4 km (γ = 0.2% at L4). Those γ values are shown in **Table 2** (note that no ash particles were detected at the L5 and L6 layer at the end of the P-MPL observational period, i.e. in week 11). In general, volcanic ash reached mostly altitudes lower than 3 km height, being undetected higher than 4 km in the last weeks of the volcano activity. Moreover, mass concentrations of ash particles (this will be addressed in more detail in **Sect. 3.3**) reached larger values than 200 μg m^{-3} (high contamination level) just above the volcano altitude (1-2 km), and at higher heights up to 5 km until the middle of the whole period (see **Fig. 7a**). Likewise, non-ash particles were also observed overcoming those high levels only at altitudes close to the volcano (1-2 km height) along the 11 weeks (see **Fig. 7b**).

3.3 Volcanic impact in the troposphere under two worst-case-scenarios (WCS)

In **Section 3.1** the potential underestimation of the mass concentrations for ash particles (m_a) by using the AERONET mass conversion factors was stated as large-to-giant particle size distributions are assumed to dominate fresh volcanic plumes (e.g. Ansmann et al., 2011; Pisani et al., 2012). In addition, it should be mentioned that the lidar signals were screened at given times by dense volcanic plumes preventing thus the retrieval of the optical properties, and then the mass determination. Hence, mass concentrations are supposed to be higher than those estimated by applying AERONET-derived conversion factors. Therefore, m_a were also derived under two extreme volcanic burden conditions, i.e. the so-called WCS (Sicard et al., 2022) as regarded in **Sect. 3.1**. That is, both WCS with assumed particle size distributions with effective radii of 4 μm (WCS1, aged-like volcanic conditions) and 10 μm (WCS2, fresh-like volcanic conditions) were also studied; those two r_{eff} values corresponded to enhancements of f_m, and hence m_a, by a factor of 3.7 (WCS1) and 9.2 (WCS2), respectively.

The goal of this section is to analyse the vertical impact of the volcanic plumes in the troposphere under those two WCS in terms of the altitudes reached by the ash particles with mass concentrations m_a higher than relevant both high and extreme mass thresholds. Indeed, the selected m_a limits of 200 (high) and 2000 (extreme) μg m^{-3} were the thresholds corresponding, respectively, to the first contamination level defined by the UK Meteorological Office after the eruption of Eyjafjallajökull volcano in 2010, and the top concentration acceptable for regular aircraft flights (ICAO, 2010; Schumann et al., 2011).

For that purpose, first, the nominal volcanic scenario was analysed. **Figure 7** shows a coloured masking defining those altitudes in height-intervals of 1 km thick (L layers), where m_a and m_{na} reached values higher than the high limit of 200 μg m^{-3} (UK Met-defined contamination level), for the overall observational P-MPL period of 11 weeks long (15 weeks from the volcanic eruption). Results indicated that the high mass threshold was sporadically overcome for ash particles at heights mostly above the volcano altitude and less than 5 km height, and before the end of observational week 5 (week 9 from the eruption) (see **Fig. 7a**), disregarding that it was shortly outpointed at 3-4 km height in week 6. Despite no contamination limits were defined for non-

ash (fine) aerosols, and just for comparison, m_{na} values prevailed over that contamination limit at random times and close to volcano altitude (mostly, no higher than 2 km height) (see **Fig. 7b**). Overcome of the extreme limit (2000 μg m^{-3}) of both the ash and non-ash mass concentrations was not observed at any altitude (data not shown).

The situation definitely changed by examining both the WCS for the ash particles. Likewise the NVS (see **Fig. 7**), **Figure 8** shows those altitudes in height-intervals of 1 km thick (L layers, coloured masking), where a potential 'enhanced' m_a for each WCS (WCS1 and WCS2 represented, respectively, by 3.7 and 9.2 times m_a enhancement) would present values higher than those of both selected high (> 200 μg m^{-3}) and extreme (> 2000 μg m^{-3}) mass thresholds.

In the case of WCS1 (see **Figs. 8a** and **8b**, top panels), ash mass concentrations overcome the contamination level (**Fig. 8a**) at heights up to 4 km mostly within week 1 (sporadically also within week 3) for the P-MPL observational period. Later on, those exceeded ash mass levels were observed at lower altitudes up to 2 km height until the beginning of week 9, although discrete 'time-gaps' with no ash contamination were also found. Regarding the extreme mass levels (> 2000 μg m^{-3}), they were overcome mostly within week 1 at 3-4 km height (**Fig. 8b**). In the case of WCS2 (see **Figs. 8c** and **8d**, bottom panels), a similar pattern to the WCS1 was found for high ash mass concentrations (**Fig. 8c**), only differentiated by observing much less those 'time-gaps'. Indeed, high m_a values were obtained up to 2 km height (close to the volcano altitude) regularly all along the observational P-MPL period; they were also observed up to 4 km height and between 2 and 5 km in week 1 and within week 3, respectively. In comparison with the WCS1, extreme m_a concentrations (> 2000 μg m^{-3}) were randomly found between the week 1 and 5 mostly up to 3-4 km height with a single event reaching 5 km height within week 3 (**Fig. 8d**). From week 6 until the end of the period (31 December 2021) extreme m_a were almost not found. However, the single event observed close to the volcano altitude within week 8 coincides in time with the increase in the total mass loading (hourly M^{total} peaked in 7567 mg m^{-2} in week 8 for the WCS2). Note that M^{total} is dominated by the mass concentration of the ash particles; indeed, weekly M^{total} values (see cyan line in **Fig. 5**) corresponded to M_a = 1283 ± 1123 mg m^{-2} in week 8 for the WCS2. Pisani et al. (2012) and Scollo et al. (2012) also used the same criterion as for WCS2 (coarse r_{eff} of 10 μm) at the source in a fresh volcanic plume of Mt. Etna volcano on 15 November 2010 with a slant lidar pointing towards the volcano vent. They found values of m_a varying between 300 and 24000 μg m^{-3}. In this case study (only measurements for one day were examined), the limit of 2000 μg m^{-3} was often largely exceeded.

In addition, the period between weeks 9 and 11 presented practically missing both high and extreme m_a values. This is due to the fact that the relative contribution of ash particles M_a^{rel} for that period was less than 20% (see **Fig. 5**). Hence, the ash mass loading was rather low (M_a = 37 ± 13 mg m^{-2}) on average for weeks 9-11; even for potential m_a enhancements of 9.2 times (note that this corresponded to fresh-like ash particles, e.g. coarse mode of the particle size distributions with r_{eff} of 10 μm; see **Sect. 3.1**), mean M_a values of 342 ± 119 mg m^{-2} were obtained for the last weeks 9-11 (8.3% with respect to week 1).

4. Summary and Conclusions

Volcanic aerosols were released to the troposphere after the eruption of the new volcano in the Cumbre Vieja Natural Park at the island of La Palma (Canary Islands) in September 2021. In this work, the mass concentrations of both the volcanic coarse and fine components (corresponding to ash and non-ash particles, respectively) were obtained by using a two-fold approach. First, the POLIPHON algorithm was applied for the separation of the optical properties (e.g. the particle backscatter coefficients) into the ash (coarse) and non-ash (fine) components by using the P-MPL observations as carried out from 17 October to the end of December 2021 (11 weeks, i.e. 15 weeks from the volcanic eruption). Second, a first approximation of the volume-to-extinction conversion factors was achieved by using the AERONET data retrieved from the sun/sky photometer measurements (from 22 September on). A statistical analysis of those factors was performed, leading to the determination of the most representative values of the mass conversion factors f_m (and the volume ones f_v)

for both ash and non-ash components under the particular volcanic conditions at La Palma Island overall. Indeed, the values of f_m^a = 1.89 $\pm$ 0.53 g m^{-2} (f_v^a = 0.726 $\pm$ 0.202 10^{-12} Mm) and f_m^{na} = 0.31 $\pm$ 0.06 (f_v^{na} = 0.204 $\pm$ 0.041 10^{-12} Mm) were estimated. Two dust episodes as observed during the observational period were discarded from the study.

Despite large-to-giant particles being assumed to be present in fresh volcanic plumes, the AERONET retrieval for particles with radii larger than 15 μm cannot be performed. This may produce an underestimation of the mass concentration of the ash particles (coarse mode dominating). This potential limitation was overcome by calculating the mass conversion factors for size distributions being dominated by coarse particles with effective radii of 4 and 10 μm, which are assumed predominant for volcanic aged-like and fresh-like particle conditions, respectively. Those values corresponded to mass enhancements of 3.7 and 9.2 times, which were represented by the so-called worst-case-scenarios (WCS1 and WCS2, respectively), in comparison with the nominal volcanic scenario (NVS, no mass enhancement). The vertical impact of volcanic aerosols was examined in terms of the altitudes reached by the ash particles with mass concentrations higher than two mass thresholds. Those limits were the first contamination level as defined by the UK Met-Office after the eruption of Eyjafjallajökull volcano in 2010 (i.e. 200 μg m^{-3}, high volcanic levels), and the maximal concentration acceptable for regular flight operation (i.e. 2000 μg m^{-3}, extreme volcanic levels). As expected, extreme ash mass concentrations were found close to the volcano altitude (1120 km height a.s.l.) for both WCS, but mainly under the WCS2 (fresh-like ash particles with effective radii of 10 μm).

In general, the ash-to-total mass loading ratio was continuously decreasing with time. However, random increases in ash particles were also observed at discrete times, likely reflecting sporadic renewals of the volcanic activity. In week 1, on average, the relative ash mass contribution was 73 $\pm$ 18%, with a total mass loading of 566 $\pm$ 281 mg m^{-2} for the nominal volcanic case, being gradually reduced down to 38 $\pm$ 32% and 120 $\pm$ 49 mg m^{-2}, respectively, within the week 11 (dust episodes were discarded). Indeed, the reduction ratio between weeks 11 and 1 of the total mass loading represented 21.2%, meanwhile the corresponding ratio for the ash mass loading was 9.8% (i.e. one order of magnitude lower with respect to those levels observed at the beginning of the observational period, that is, after the last 11 weeks of eruptive activity).

The troposphere was dominated by ash particles (> 80% predominance in the total atmospheric column) around 11 % out of the overall observational period (11 weeks). The reduction ratio decreased with increasing layer height, i.e. from around 19% between the surface and 1 km height until almost zero at 3-4 km (no ash particles were observed above). Regarding air quality concerns on volcanic fine contaminants, and despite no contamination limits were defined for non-ash (fine) particles, they were also observed overcoming the high contamination levels (> 200 μg m^{-3}) only at heights close to the volcano altitude (i.e. 1-2 km) along the whole period.

The vertical impact of the volcanic plumes in the troposphere can be considered relevant for both WCS by exceeding the high contamination levels mostly within week 1 (week 5 from the volcanic eruption), reaching altitudes up to 5-6 km height. Those altitudes were lower, mostly close to the volcano altitude (1-2 km), later on (until week 9, i.e. week 13 from the volcanic eruption), with no effect until the end of the observational period. In relation to overcoming the extreme mass levels (linked to aircraft flight limitations), the volcano activity became irrelevant during the whole period and for the last 5 weeks, respectively, under WCS1 and WCS2 conditions.

Therefore, the estimation of the mass concentration of volcanic matter relies on an accurate determination of the mass conversion factors; this is highly required for both air quality concerns and air traffic regulation and safety issues. Indeed, reporting volcanic mass concentrations in near real-time is linked to obtaining a validated parameterization of mass conversion factors. This parametrization depends especially on the transport duration of the volcanic ash and the type of volcanic eruption. In particular, due to the high correlation between the mass conversion factor and the effective particle size, it would be necessary to

565 determine the size distribution of the ash particles once emitted by the volcano and its potential changes during their short- and long-range transport.

The relevance of this study lies in the application of the exposed methodology for investigating the release of ash particles to the atmosphere in future volcanic eruptions in relation to established warning systems of
570 extreme events. In addition, this work infers a new long-term insight on the volcanic matter injected into the atmosphere with relevance for Air Quality issues and air traffic safety policies.

CRediT authorship contribution statement

575 **Carmen Córdoba-Jabonero:** Conceptualization, Methodology, Software, Formal analysis, Investigation, Data curation, Writing-original draft preparation, Writing—review and editing, Supervision, funding acquisition. **Michaël Sicard:** Conceptualization, Methodology, Formal analysis, Investigation, Data curation, Writing—review and editing, Supervision, funding acquisition. **África Barreto:** Conceptualization, Investigation, Resources, Data curation, Writing—review and editing. **Carlos Toledano:** Resources, Data curation, Writing—
580 review and editing. **María Ángeles López-Cayuela:** Writing—review and editing. **Cristina Gil-Díaz:** Writing—review and editing. **Omaira García:** Writing—review and editing, Funding acquisition. **Clara Violeta Carvajal-Pérez:** Writing—review and editing. **Adolfo Comerón:** Writing—review and editing. **Ramón Ramos:** Resources, Writing—review and editing. **Constantino Muñoz-Porcar:** Writing—review and editing. **Alejandro Rodríguez-Gómez:** Writing—review and editing.

585

Acknowledgements

The authors acknowledge the extraordinary effort carried out by the AEMET staff (both in La Palma and in support of the activites in La Palma) during the volcanic eruption, from the Izaña Atmospheric Research Center and the Delegation of AEMET in the Canary Islands. We also gratefully acknowledge the dedication and
590 information provided by the PEVOLCA Scientific Committee and all the support received from the insular and local governments (Cabildo Insular de La Palma and the Ayuntamientos de Tazacorte and Fuencaliente). This research was funded by the Spanish Ministry of Science and Innovation (PID2020-118793GA-I00, PID2019-104205GB-C21/AEI/10.13039/501100011033, PID2019-103886RB-I00, EQC2018-004686-P) and the Unit of Excellence "María de Maeztu" (MDM-2017-0737) and ACTRIS-Spain (CGL2017-90884-REDT) by the Spanish
595 State Research Agency (AEI). The authors wish to thank the support from the H2020 program of the European Union and ACTRIS (GA n. 19ENV04, 654109, 778349, 871115, 101008004, and 101086690), and the European components of AERONET acting in the frame of ACTRIS RI, and also AEROSPAIN and Junta de Castilla y León (VA227P20) for supporting the calibration of the AERONET sun photometer used in this publication. M.Á.L.-C. and C.V.C.-P. are supported by the INTA predoctoral contract program. J. E. Welton and S. Stewart at NASA
600 GSFC are acknowledged for their continuous help in keeping the MPL systems and the data analysis up to date.

Data Availability

The data used in this work are also used in other ongoing studies about the transport of the volcanic plume and are not public at the moment. They can be obtained upon request from the corresponding author.

605

Conflicts of Interest

The authors declare no conflict of interest.

References

610

ACTRIS (https://actris.es.webstsc.webs.upc.edu/en/node/11; last access: 17 December 2021).

AERONET (https://aeronet.gsfc.nasa.gov; last access: 17 January 2022).

Ansmann A., Tesche, M., Seifert, P., Groß, S., Freudenthaler, V., Apituley, A., Wilson, K.M., Serikov, I., Linné, H., Heinold, B., 2011. Ash and fine mode particle mass profiles from EARLINET-AERONET observations over central Europe after the eruptions of the Eyjafjallajökull volcano in 2010. J. Geophys. Res.-Atmos. 116(D20). https://doi.org/10.1029/2010JD015567.

Ansmann, A., Seifert, P., Tesche, M., Wandinger, U., 2012. Profiling of fine and coarse particle mass: case studies of Saharan dust and Eyjafjallajökull/Grimsvötn volcanic plumes. Atmos. Chem. Phys. 12(20), 9399–9415. https://doi.org/10.5194/acp-12-9399-2012.

Bedoya-Velásquez, A.E.; Hoyos-Restrepo, M.; Barreto, A.; García, R.D.; Romero-Campos, P.M.; García, O.; Ramos, R.; Roininen, R.; Toledano, C.; Sicard, M.; Ceolato, R., 2022. Estimation of the Mass Concentration of Volcanic Ash Using Ceilometers: Study of Fresh and Transported Plumes from La Palma Volcano. Remote Sens. 14, 5680. https://doi.org/10.3390/rs14225680.

Campbell, J.R., Hlavka, D.L., Welton, E.J., Flynn, C.J., Turner, D.D., Spinhirne, J.D., Scott, V.S., Hwang, I.H., 2002. Full-Time, Eye-Safe Cloud and Aerosol Lidar Observation at Atmospheric Radiation Measurement Program Sites: Instruments and Data Processing. J. Atmos. Ocean. Technol. 19(4), 431–442. https://doi.org/10.1175/1520-0426(2002)019<0431:FTESCA>2.0.CO,2.

Colette, A., Favez, O., Meleux, F., Chiappini, L., Haeffelin, M., Morille, Y., Malherbe, L., Papin, A., Bessagnet, B., Menut, L., Leoz, E., Rouïl, L., 2011. Assessing in near real time the impact of the April 2010 Eyjafjallajökull ash plume on air quality. Atmos. Environ. 45(5), 1217-1221. https://doi.org/10.1016/j.atmosenv.2010.09.064.

Córdoba-Jabonero, C., Sicard, M., Ansmann, A., Águila, A., Baars, H., 2018. Separation of the Optical and Mass Features of Particle Components in Different Aerosol Mixtures by Using POLIPHON Retrievals in Synergy with Continuous Polarized Micro-Pulse Lidar (P-MPL) Measurements. Atmos. Meas. Tech. 11(8), 4775–4795. https://doi.org/10.5194/amt-11-4775-2018.

Córdoba-Jabonero, C., Ansmann, A., Jiménez, C., Baars, H., López-Cayuela, M.-Á., Engelmann, R., 2021. Experimental Assessment of a Micro-Pulse Lidar System in Comparison with Reference Lidar Measurements for Aerosol Optical Properties Retrieval. Atmos. Meas. Tech. 14(7), 5225–5239. https://doi.org/10.5194/amt-14-5225-2021.

Europa Press (https://www.europapress.es/islas-canarias/noticia-canarias-remite-gobierno-evaluacion-danos-volcan-palma-84233-millones-20211204160648.html, last access: 04 December 2021).

Felpeto, A., Molina-Arias, A. J., Quirós, F., Pereda, J., García-Cañada, L., and Díaz-Suárez, E. A., 2022. Measuring the height of the eruptive column during the 2021 eruption of Cumbre Vieja (La Palma Island, Canary Islands). EGU General Assembly Conference Abstracts, EGU22-9419, https://doi.org/10.5194/egusphere-egu22-9419.

Fernald, F. G., 1984. Analysis of Atmospheric Lidar Observations: Some Comments. Appl. Optics. 23, 652–653. https://doi.org/10.1364/AO.23.000652.

Flynn, C.J., Mendoza, A., Zheng, Y., Mathur, S., 2007. Novel Polarization-Sensitive Micropulse Lidar Measurement Technique. Opt. Express. 15(6), 2785–2790. https://doi.org/10.1364/OE.15.002785.

García, O., Suárez, D., Cuevas, E., Ramos, R., Barreto, Á., Hernández, M., Quintero, V., Toledano, C., Sicard, M., Córdoba-Jabonero, C., Riz, V., Roininen, R., López, C., Vilches, J., Weiss, M., Carreño, V., Taquet, N., Boulesteix, T., Fraile, E., Torres, C., Prats, N., Alcántara, A., León, S., Rivas, P., Álvarez, Ó., Parra, F., de Luis, J., González, C., Armas, C., Romero, P., de Bustos, J., Redondas, A., Marrero, C., Milford, C., Román, R., González, R., López-Cayuela, M., Carvajal-Pérez, C., Chinea, N., García, R., Almansa, F., González, Y., Bullón, F., Poggio, M., Rivera,

C., Bayo, C., Rey, F., 2022. La erupción volcánica de La Palma y el papel de la Agencia Estatal de Meteorología. Revista Tiempo Y Clima, 5(76). https://pub.ame-web.org/index.php/TyC/article/view/2516.

Gasteiger, J., Groß, S., Freudenthaler, V., Wiegner, M., 2011. Volcanic ash from Iceland over Munich: Mass concentration retrieved from ground-based remote sensing measurements. Atmos. Chem. Phys. 11(5), 2209–2223. https://doi.org/10.5194/acp-11-2209-2011.

Giles, D. M., Sinyuk, A., Sorokin, M. G., Schafer, J. S., Smirnov, A., Slutsker, I., Eck, T. F., Holben, B. N., Lewis, J. R., Campbell, J. R., Welton, E. J., Korkin, S. V., and Lyapustin, A. I., 2019. Advancements in the Aerosol Robotic Network (AERONET) Version 3 database – automated near-real-time quality control algorithm with improved cloud screening for Sun photometer aerosol optical depth (AOD) measurements. Atmos. Meas. Tech. 12, 169–209. https://doi.org/10.5194/amt-12-169-2019.

Hervo, M., Quennehen, B., Kristiansen, N. I., Boulon, J., Stohl, A., Fréville, P., Pichon, J.-M., Picard, D., Labazuy, P., Gouhier, M., Roger, J.-C., Colomb, A., Schwarzenboeck, A., Sellegri, K., 2012. Physical and optical properties of 2010 Eyjafjallajökull volcanic eruption aerosol: Ground-based, Lidar and airborne measurements in France. Atmos. Chem. Phys. 12(4), 1721–1736. https://doi.org/10.5194/acp-12-1721-2012.

Holben, B.N., Eck, T.F., Slutsker, I., Tanré, D., Buis, J.P., Setzer, A., Vermote, E., Reagan, J.A., Kaufman, Y.J., Nakajima, T., Lavenu, f., Jankowiak, I., Smirnov, A., 1998. AERONET—A Federated Instrument Network and Data Archive for Aerosol Characterization. Remote Sens. Environ. 66(1), 1-16. https://doi.org/10.1016/S0034-4257(98)00031-5.

Icelandic Directorate of Health (https://www.landlaeknir.is/english/annual-reports/, last access: 25 January 2023).

Klett, J. D., 1985. Lidar Inversion with Variable Backscatter/Extinction Ratios. Appl. Optics. 24(11), 1638–1643. https://doi.org/10.1364/AO.24.001638.

Kokkalis, P., Papayannis, A., Amiridis, V., Mamouri, R. E., Veselovskii, I., Kolgotin, A., Tsaknakis, G., Kristiansen, N. I., Stohl, A., Mona, L., 2013. Optical, microphysical, mass and geometrical properties of aged volcanic particles observed over Athens, Greece, during the Eyjafjallajökull eruption in April 2010 through synergy of Raman lidar and sunphotometer measurements. Atmos. Chem. Phys. 13(18), 9303–9320. https://doi.org/10.5194/acp-13-9303-2013.

Lathem, T.L., Kumar, P., Nenes, A., Dufek, J., Sokolik, I.N., Trail, M., Russell, A., 2011. Hygroscopic properties of volcanic ash. Geophys. Res. Lett. 38(11), L11802. https://doi.org/10.1029/2011GL047298.

Longpré, M.-A., 2021. Reactivation of Cumbre Vieja volcano. Science. 374(6572), 1197–1198. https://doi.org/10.1126/science.abm9423.

Lopes, F.J.S., Silva, J.J., Antuña Marrero, J.C., Taha, G., Landulfo, E., 2019. Synergetic Aerosol Layer Observation After the 2015 Calbuco Volcanic Eruption Event. Remote Sens. 11(2), 195. https://doi.org/10.3390/rs11020195.

Mattis, I., Seifert, P., Müller, D., Tesche, M., Hiebsch, A., Kanitz, T., Schmidt, J., Finger, F.,Wandinger, U., Ansmann, A., 2010. Volcanic aerosol layers observed with multiwavelength Raman lidar over central Europe in 2008–2009. J. Geophys. Res.-Atmos. 115(D2), D00L04. https://doi.org/10.1029/2009JD013472.

Milford, C., Torres, C., Vilches, J., Gossman, A-K., Weis, F., Suárez-Molina, D., García, O.E., Prats, N., Barreto, A., García, R.D., Bustos, J.J., Marrero, C.L., Ramos, R., Chinea, N., Boulesteix, T., Taquet, N., Rodríguez, S., López-Darias, J., Sicard, M., Córdoba-Jabonero, C., Cuevas, E., 2023. Impact of the 2021 La Palma volcanic eruption

on air quality: insights from a multidisciplinary approach, Science of The Total Environment, 869, 161652. https://doi.org/10.1016/j.scitotenv.2023.161652.

Mona, L., Amodeo, A., D'Amico, G., Giunta, A., Madonna, F., Pappalardo, G., 2012. Multi-wavelength Raman lidar observations of the Eyjafjallajökull volcanic cloud over Potenza, southern Italy. Atmos. Chem. Phys. 12(4), 2229–2244. https://doi.org/10.5194/acp-12-2229-2012.

Navas-Guzmán, F., Müller, D., Bravo-Aranda, J.A., Guerrero-Rascado, J.L., Granados-Muñoz, M.J., Pérez-Ramírez, D., Olmo, F.J., Alados-Arboledas, L., 2013. Eruption of the Eyjafjallajökull Volcano in spring 2010: Multiwavelength Raman lidar measurements of sulphate particles in the lower troposphere. J. Geophys. Res.-Atmos. 118(4), 1804–1813. https://doi.org/10.1002/jgrd.50116.

Newhall, C.G., Self, S., 1982. The volcanic explosivity index (VEI) an estimate of explosive magnitude for historical volcanism. J. Geophys. Res.-Ocean. 87(C2), 1231-1238. https://doi.org/10.1029/JC087iC02p01231.

Papayannis, A., Mamouri, R.E., Amiridis, V., Giannakaki, E., Veselovskii, I., Kokkalis, P., Tsaknakis, G., Balis, D., Kristiansen, N.I., Stohl, A., Korenskiy, M., Allakhverdiev, K., Huseyinoglu, M. F., Baykara, T., 2012. Optical properties and vertical extension of aged ash layers over the Eastern Mediterranean as observed by Raman lidars during the Eyjafjallajökull eruption in May 2010. Atmos. Environ. 48, 56–65. https://doi.org/10.1016/j.atmosenv.2011.08.037.

Pappalardo, G., Amodeo, A., Apituley, A., Comeron, A., Freudenthaler, V., Linné, H., Ansmann, A., Bösenberg, J., D'Amico, G., Mattis, I., Mona, L., Wandinger, U., Amiridis, V., Alados-Arboledas, L., Nicolae, D., Wiegner, M., 2014. EARLINET: Towards an advanced sustainable European aerosol lidar network. Atmos. Meas. Tech. 7(8), 2389–2409. https://doi.org/10.5194/amt-7-2389-2014.

PEVOLCA (https://info.igme.es/eventos/Erupcion-volcanica-la-palma/pevolca, last access: 17 December 2021).

Pisani, G., Boselli, A., Coltelli, M., Leto, G., Pica, G., Scollo, S., Spinelli, N.,Wang, X., 2012. Lidar depolarization measurement of fresh volcanic ash from Mt. Etna, Italy. Atmos. Environ. 2012, 62, 34–40. https://doi.org/10.1016/j.atmosenv.2012.08.015.

Prata, A.J., Prata, A.T., 2012. Eyjafjallajökull volcanic ash concentrations determined using Spin Enhanced Visible and Infrared Imager measurements. J. Geophys. Res.-Atmos. 117(D20). https://doi.org/10.1029/2011JD016800.

Prata, A.T., Young, S.A., Siems, S.T., Manton, M.J., 2017. Lidar ratios of stratospheric volcanic ash and sulfate aerosols retrieved from CALIOP measurements. Atmos. Chem. Phys. 17(13), 8599–8618. https://doi.org/10.5194/acp-17-8599-2017.

Robock, A., 2000. Volcanic Eruptions and Climate. Rev. Geophys. 38(2), 191-219. https://doi.org/10.1029/1998RG000054.

Robock, A., and C. Oppenheimer (Eds.), 2003. Volcanism and the Earth's Atmosphere, Geophysical Monograph 139, American Geophysical Union, Washington, DC, 360 pp.

Sannino, A., Amoruso, S., Damiano, R., Scollo, S., Sellitto, P., Boselli, A., 2022. Optical and microphysical characterization of atmospheric aerosol in the Central Mediterranean during simultaneous volcanic ash and desert dust transport events. Atmos. Res. 271, 106099. https://doi.org/10.1016/j.atmosres.2022.106099.

Sawamura, P., Vernier, J.P., Barnes, J.E., Berkoff, T.A., Welton, E.J., Alados-Arboledas, L., Navas-Guzmán, F., Pappalardo, G., Mona, L., Madonna, F., Lange, D., Sicard, M., Godin-Beekmann, S., Payen, G., Wang, Z., Hu, S., Tripathi, S.N., Cordoba-Jabonero, C., Hoff, R.M., 2012. Stratospheric AOD after the 2011 eruption of Nabro volcano measured by lidars over the Northern Hemisphere. Environ. Res. Lett. 7(3), 034013. https://doi.org/10.1088/1748-9326/7/3/034013.

Scollo, S., Boselli, A., Coltelli, M., Leto, G., 2012. Monitoring Etna volcanic plumes using a scanning LiDAR. Bull. Volcanol. 74(10), 2383–2395. https://doi.org/10.1007/s00445-012-0669-y.

Sicard, M., Guerrero-Rascado, J.L., Navas-Guzmán, F., Preißler, J., Molero, F., Toms, S., Bravo-Aranda, J.A., Comerón, A., Rocadenbosch, F., Wagner, F., Pujadas, M., Alados-Arboledas, L., 2012. Monitoring of the Eyjafjallajökull volcanic aerosol plume over the Iberian Peninsula by means of four EARLINET lidar stations. Atmos. Chem. Phys. 12(6), 3115–3130. https://doi.org/10.5194/acp-12-3115-2012.

Sicard, M., Córdoba-Jabonero, C., Barreto, A., Welton, E.J., Gil-Díaz, C., Carvajal-Pérez, C.V., Comerón, A., García, O., García, R., López-Cayuela, M.-Á., Muñoz-Porcar, C., Prats, N., Ramos, R., Rodríguez-Gómez, A., Toledano, C., Torres, C., 2022. Volcanic Eruption of Cumbre Vieja, La Palma, Spain: A First Insight to the Particulate Matter Injected in the Troposphere. Remote Sens. 14(10), 2470. https://doi.org/10.3390/rs14102470.

Sinyuk, A., Holben, B. N., Eck, T. F., Giles, D. M., Slutsker, I., Korkin, S., Schafer, J. S., Smirnov, A., Sorokin, M., and Lyapustin, A., 2020. The AERONET Version 3 aerosol retrieval algorithm, associated uncertainties and comparisons to Version 2. Atmos. Meas. Tech. 13, 3375–3411. https://doi.org/10.5194/amt-13-3375-2020.

Schumann, U., Weinzierl, B., Reitebuch, O., Schlager, H., Minikin, A., Forster, C., Baumann, R., Sailer, T., Graf, K., Mannstein, H., Voigt, C., Rahm, S., Simmet, R., Scheibe, M., Lichtenstern, M., Stock, P., Rüba, H., Schäuble, D., Tafferner, A., Rautenhaus, M., Gerz, T., Ziereis, H., Krautstrunk, M., Mallaun, C., Gayet, J.-F., Lieke, K., Kandler, K., Ebert, M., Weinbruch, S., Stohl, A., Gasteiger, J., Gross, S., Freudenthaler, V., Wiegner, M., Ansmann, A., Tesche, M., Olafsson, H., Sturm, K., 2011. Airborne observations of the Eyjafjalla volcano ash cloud over Europe during air space closure in April and May 2010. Atmos. Chem. Phys. 11(5), 2245–2279. https://doi.org/10.5194/acp-11-2245-2011.

Stewart, C., Damby, D.E., Horwell, C.J., Elias, T., Ilyinskaya, E., Tomasek, I., Longo, B.M., Schmidt, A., Carlsen, H.K., Mason, E., Baxter, P.J., Cronin, S., Witham, C., 2021. Volcanic air pollution and human health: recent advances and future directions. Bull. Volcanology. 84(1), 1-25. https://doi.org/10.1007/s00445-021-01513-9.

Toledano, C., Bennouna, Y., Cachorro, V., de Galisteo, J. P. O.,Stohl, A., Stebel, K., Kristiansen, N. I., Olmo, F. J., Lya-mani, H., Obregon, M. A., Estelles, V., Wagner, F., Baldasano, J. M., Gonzalez-Castanedo, Y., Clarisse, L., de Frutos, A. M., 2012. Aerosol properties of the Eyjafjallajökullash derived from sun photometer and satellite observations over the Iberian Peninsula. Atmos. Environ. 48, 22–32. https://doi.org/10.1016/j.atmosenv.2011.09.072.

Volcanic Ashfall Impact Working Group (https://volcanoes.usgs.gov/volcanic_ash/ash_clouds_air_routes_eyjafjallajokull.html, last access: 2 February 2023).

Welton, E.J., Campbell, J.R., Spinhirne, J.D., Scott III, V.S., 2001. Global monitoring of clouds and aerosols using a network of micropulse lidar systems., in: Lidar Remote Sensing for Industry and Environment Monitoring, 4153. International Society for Optics and Photonics. pp. 151–158. https://doi.org/https://doi.org/10.1117/12.417040.

Welton, E.J., Campbell, J.R., 2002. Micropulse Lidar Signals: Uncertainty Analysis. J. Atmos. Ocean. Technol., 19(12), 2089–2094. https://doi.org/10.1175/1520-0426(2002)019<2089:MLSUA>2.0.CO;2.

820

Table 1. Specific values of the PDR (δ), lidar ratio (S, sr), particle density (ρ, g cm^{-3}), and both volume (f_v, 10^{-12} Mm) and mass (f_m, g m^{-2}) conversion factors to both *a* and *na* components as introduced in the POLIPHON algorithm.

Volcanic component	Ash (*a*, coarse)	Non-ash (*na*, fine)	References
δ	0.36	0.01	Ansmann et al. (2011)
S	50	50	Ansmann et al. (2011)
ρ	2.6	1.5	Ansmann et al. (2011)
f_v	0.726 ± 0.202	0.204 ± 0.041	This work (**Sect. 3.1**)
f_m	1.89 ± 0.53	0.31 ± 0.06	This work (**Eq. 2**)

Table 2. Time percentage with respect to the overall P-MPL measurement period when the relative ash mass contribution to the total mass loading (M_a^{rel}, %) fulfils the conditions: M_a^{rel} > 80% (restrictive) and M_a^{rel} = 40-60% (less restrictive). In addition, the reduction ratio between weeks 11 and 1 (γ, %) is also included.

Layer	> 80%	40-60%	γ (%)
L1: 0-1 km	11.8	25.7	18.7
L2: 1-2 km	14.6	25.9	11.7
L3: 2-3 km	12.1	24.7	3.4
L4: 3-4 km	7.1	12.4	0.2
L5: 4-5 km (*)	3.8	1.9	--
L6: 5-6 km (*)	1.9	0.9	--
L1-L6: 0-6 km	11.0	35.2	9.8

(*) Note that no ash particles were detected at those specific layers from the middle of the P-MPL observational period on.

Figure 1. The geographical composition of the volcanic area in the Cumbre Vieja Natural Park at La Palma (Canary Islands), where the location of the new volcano formed after the eruption (red), Tazacorte (blue), Fuencaliente (purple) and the airport (green) together with their relative distances are shown. Credits: https://earth.google.com/. Insert shows the geographical position of the Canary Islands (red star, from Google Maps).

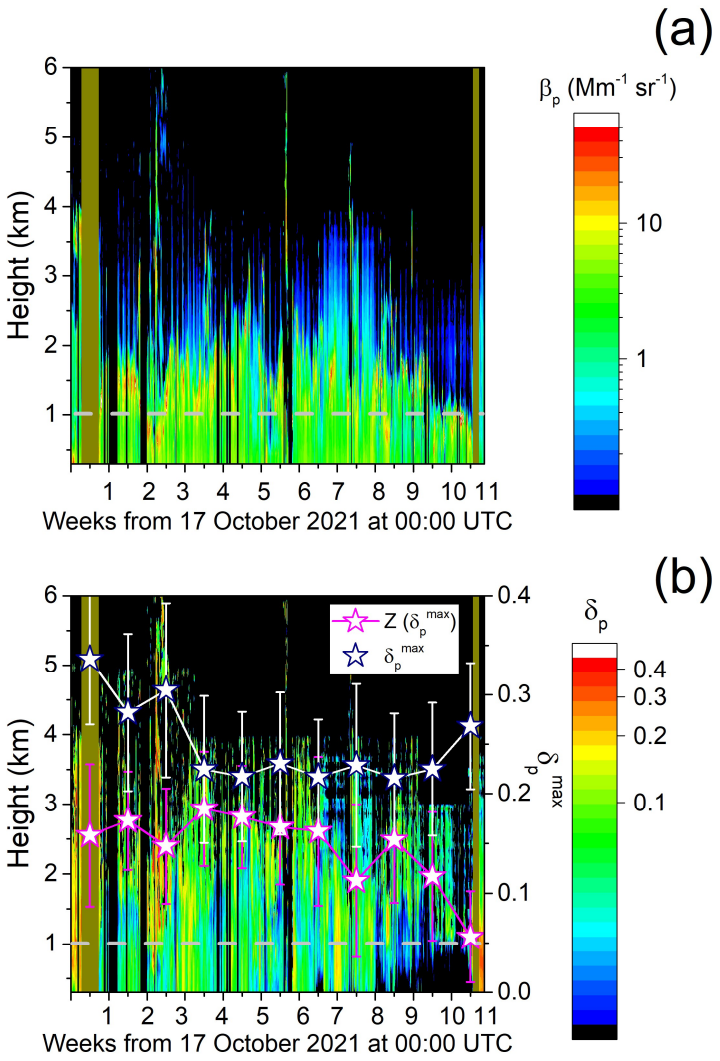

Figure 2. The evolution of the volcanic aerosols in terms of their optical properties: (a) the particle backscattering coefficient (β_p, Mm^{-1} sr^{-1}), and (b) the particle linear depolarization ratio (δ_p, PDR) along the P-MPL observational period until the end of the volcanic activity (11 weeks, from 17 October to 31 December 2021). Weekly values (and standard deviations) of the maximal PDR (δ_p^{max}, dark blue stars) together with the heights at which those values were reached ($Z(\delta_p^{max})$, magenta stars) are also shown. Volcano altitude is marked by a grey dashed line. Light brown bands indicate the dusty episodes.

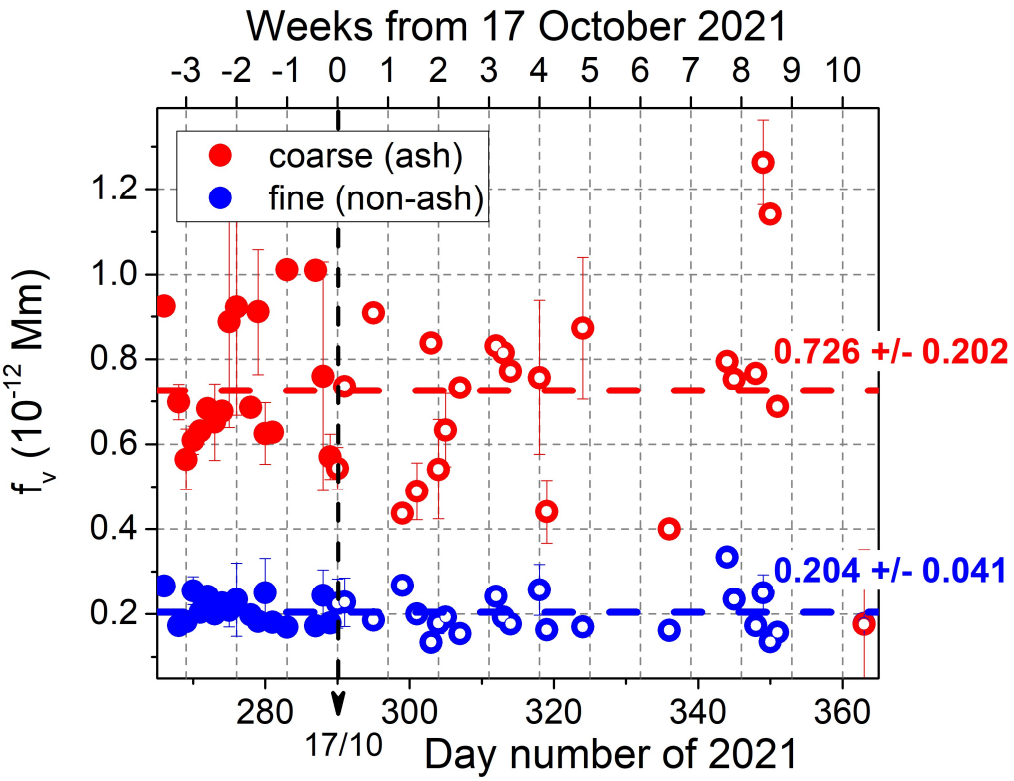

Figure 3. Evolution of the daily-averaged AERONET-based volume conversion factors (f_v) (and their standard deviations) for the fine (blue) and coarse (red) modes for the whole period from 22 September 2021 (day number = 265) to 31 December 2021 (day number = 365). The starting date of the P-MPL observations (17 October, '17/10') is marked by a black dashed arrow (white-coloured symbols highlight this shorter period), and the number of week with respect to that day is shown at the top.

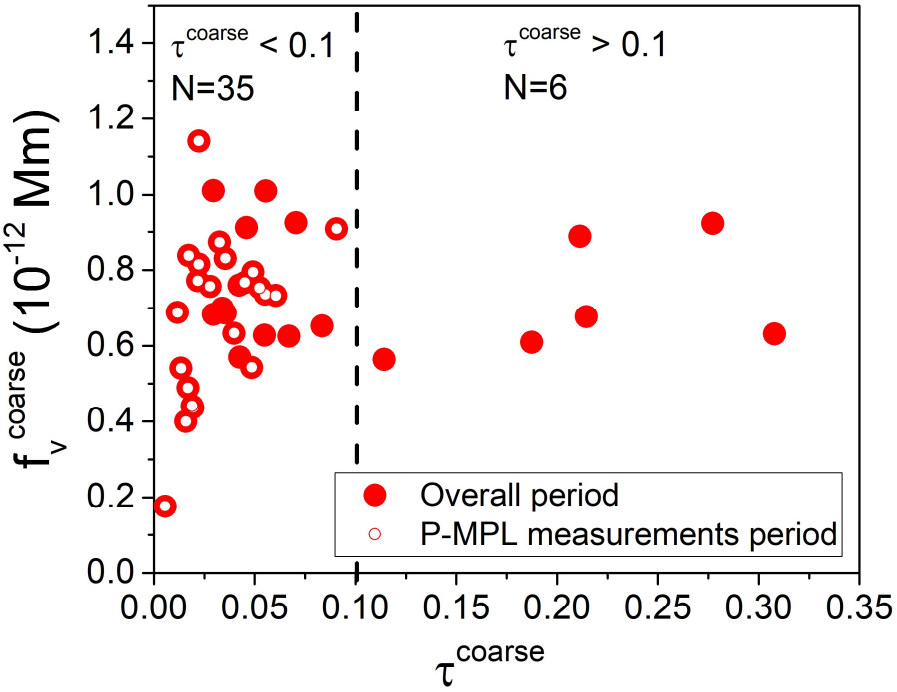

880 **Figure 4.** Coarse particles: AERONET volume conversion factor ($\boldsymbol{f_v}$) versus aerosol optical depth at 500 nm ($\boldsymbol{\tau}$) for the whole period from 22 September to 31 December 2021. White-coloured symbols highlight the partial dataset corresponding to the period starting from the P-MPL observations (17 October on). The dashed line indicates the delimitation of $\boldsymbol{\tau^{coarse}}$ = 0.1.

885

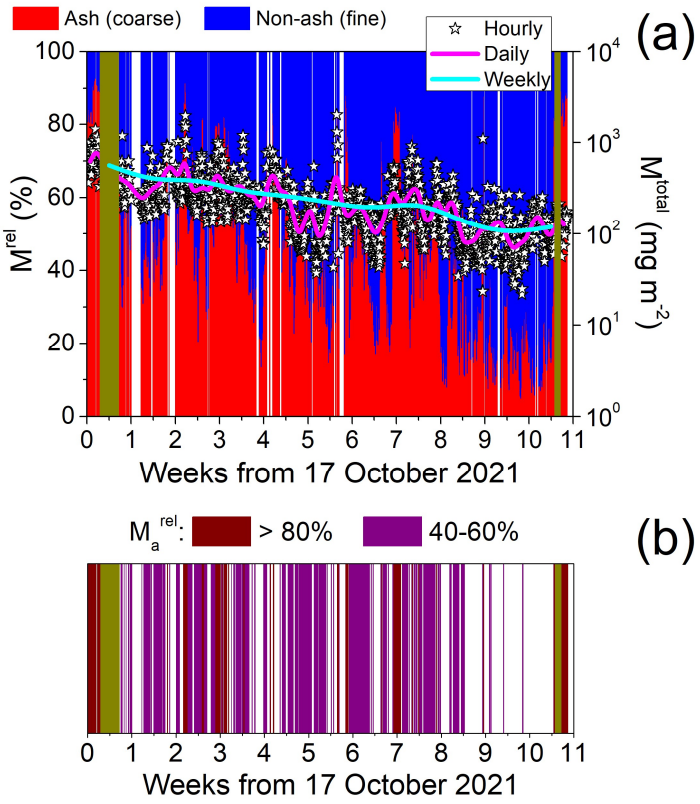

890 **Figure 5.** (a) Evolution of the ash (*a*) and non-ash (*na*) particles along the P-MPL observational period in terms of: (Left axis) Relative mass contribution ($M_i^{rel} = {M_i}/{M^{total}}$, %) with i = *a* (red) and *na* (blue); and (Right axis) the total mass loading (M^{total}, g m^{-2}), as represented by its hourly- (stars symbols), daily- (magenta line) and weekly-averaged (cyan line) values. Light brown bands mark the dusty episodes. (b) Time intervals when M_a^{rel} is higher than 80% (brown bands) and in the 40-60% range (purple bands).

895

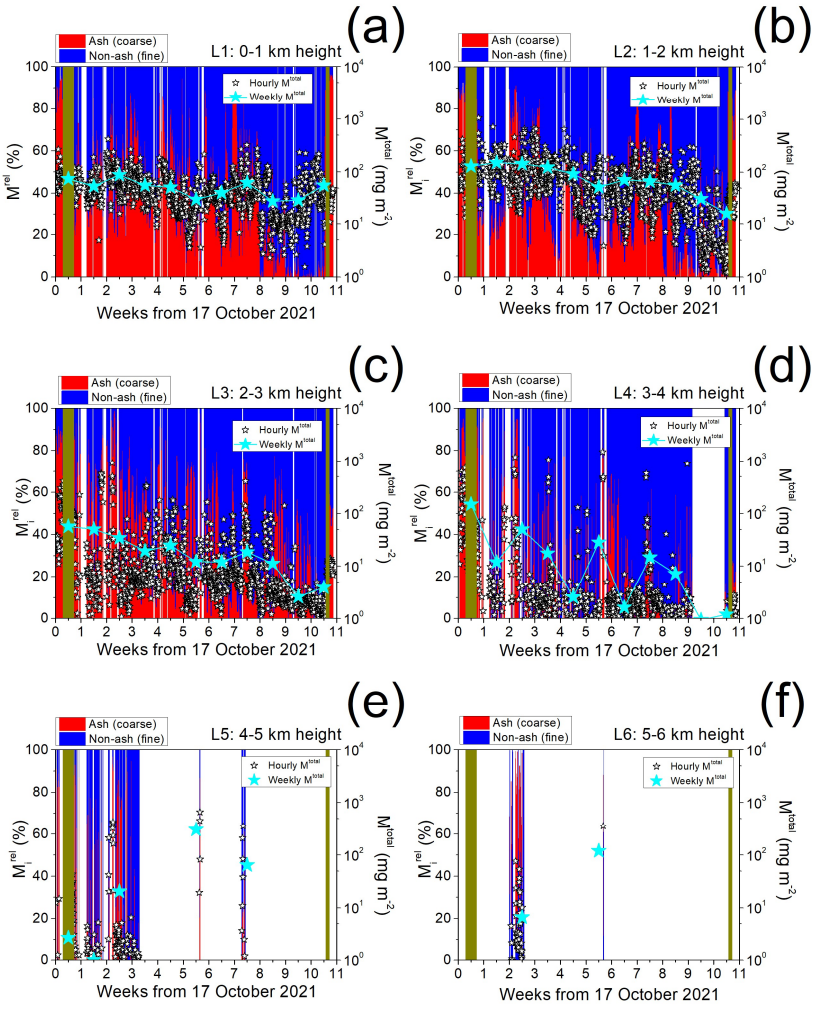

Figure 6. The same as **Fig. 5**, but the height-integration is for height-intervals of 1 km thick (L layers) up to 6 km height (see the legend in each panel) for the ash (*a*, red) and non-ash (*na*, blue) particles along the P-MPL observational period. Stars stand for the total mass loading (M^{total}, mg m^{-2}) in those discrete layers (L): white and cyan stars denote, respectively, hourly and weekly values. White bands indicate no data retrieved. Light brown bands mark the dusty episodes.

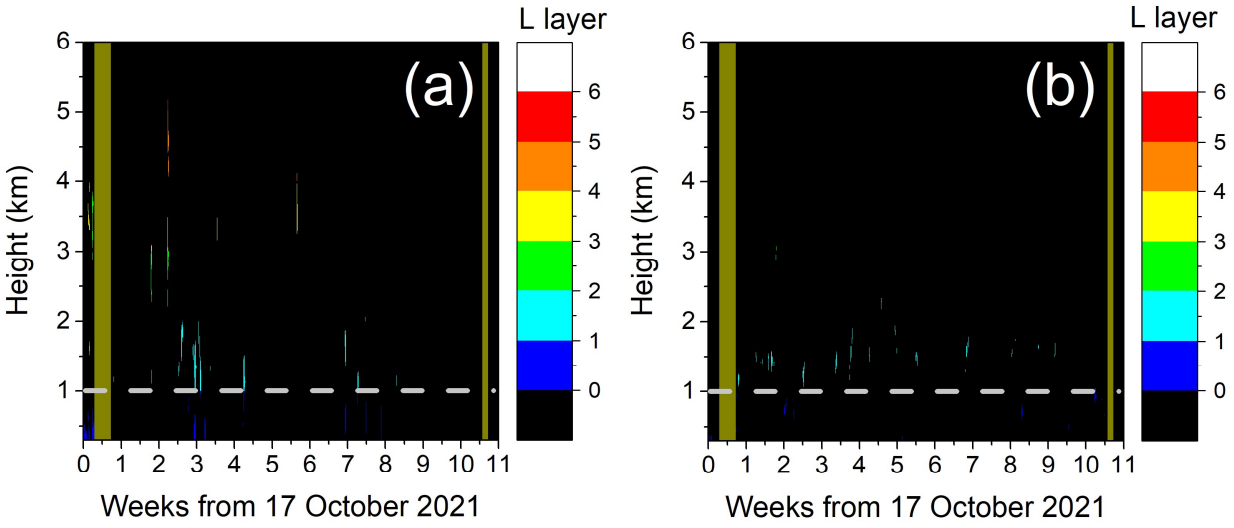

Figure 7. Nominal volcanic scenario (NVS). Coloured masking for altitudes reached by the (a) ash and (b) non-ash particles where their mass concentrations were higher than 200 μg m^{-3} (UK Met-defined first contamination level). The colour code applies to height-intervals of 1 km thick (L layers). Volcano altitude is marked by a grey dashed line. Light brown bands indicate dusty episodes.

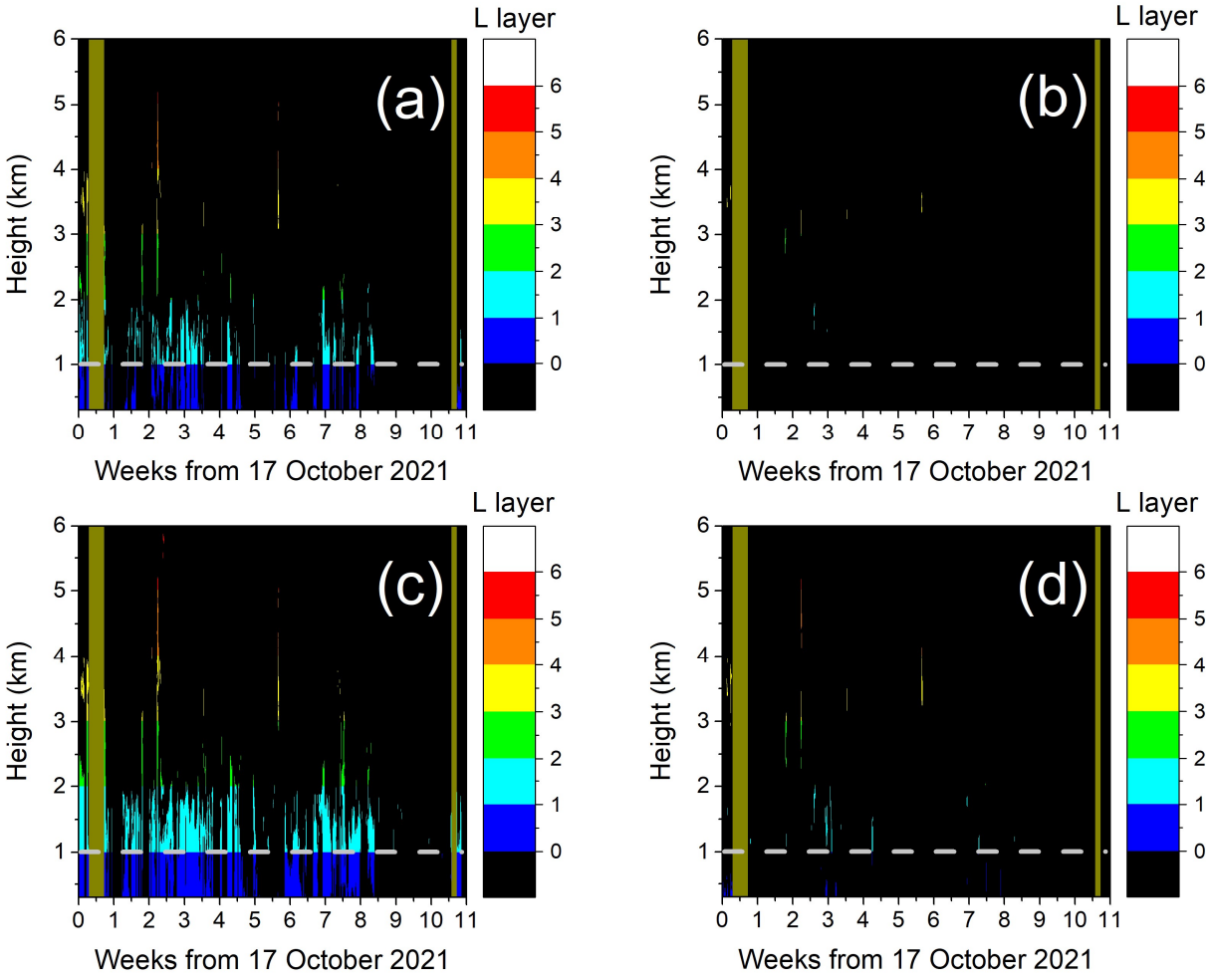

Figure 8. Worst-case-scenarios (WCS). (Top panels, a) and b) WCS1 (aged-like volcanic conditions) and (Bottom panels, c) and d) WCS2 (fresh-like volcanic conditions). Coloured masking for altitudes reached by the ash particles where their mass concentrations (m_a) were larger than (Left panels) 200 μg m^{-3} (UK Met-defined first volcanic contamination level; high-level events) and (Right panels) 2000 μg m^{-3} (volcanic threshold limit for regular air traffic; extreme-level events). Those altitudes are shown in height-intervals of 1 km thick (L layers). Volcano altitude is marked by a grey dashed line. Light brown bands indicate dusty episodes.